Arabian Journal of Chemistry (2019) **12**, 5111–5119

King Saud University

Arabian Journal of Chemistry

www.ksu.edu.sa
www.sciencedirect.com

ORIGINAL ARTICLE

Electromagnetic attributes a dominant factor for the enhanced EMI shielding of PANI/ $Li_{0.5}Fe_{2.5-x}Gd_xO_4$ core shell structured nanomaterial

M. Abdullah Dar [a,*], Kowsar Majid [a,*], M. Farukh [b], S.K. Dhawan [b], R.K. Kotnala [b], Jyoti Shah [b]

[a] *Department of Chemistry, National Institute of Technology Srinagar, Hazratbal, Srinagar 190006, India*
[b] *National Physical Laboratory (CSIR), Dr. K.S. Krishnan Road, New Delhi 110012, India*

Received 21 September 2016; accepted 3 December 2016
Available online 22 December 2016

KEYWORDS

PANI;
Nano-ferrites;
Magnetic properties;
Dielectric properties;
EMI shielding

Abstract A core-shell structured PANI/$Li_{0.5}Fe_{2.5-x}Gd_xO_4$ ($0.0 \leqslant x \leqslant 0.2$) nanocomposite material has been prepared by in situ emulsion polymerization method as is evidenced by X-ray diffraction and Scanning electron microscopy. Transmission electron microscopy confirms the formation of core (ferrite)-shell (PANI matrix) structured nanocomposite material. These materials have been investigated for electromagnetic interference (EMI) shielding in the X-band (8–12 GHz) frequency range. Higher shielding effectiveness (SE_T) of around 42 dB has been obtained in this study than many other systems reported recently. The main contributing factor has been ascribed to the absorption (SE_A = 34–36 dB) instead of reflection (SE_R = 4.0–6.3 dB), owing to the enhancement in the electromagnetic attributes. Effect of increasing Gd^{3+} ion content in PANI/$Li_{0.5}Fe_{2.5-x}Gd_xO_4$ nano-composite has been analyzed for the electromagnetic attenuation. It depicts a decreasing trend of SE with Gd^{3+} doping except for $x = 0.2$ sample. This has been attributed to the increasing particle size of ferrites, resulting into the decrease in dielectric (ε' = 59–56 at 9.5 GHz) attributes owing to increased grain to grain contact. Higher value of SE for $x = 0.2$ sample can be due to the secondary phase formation in ferrite, which increases the number of grain boundaries and thereby increases ε'. However, increasing magnetization with Gd^{3+} doping is less likely a factor affecting

* Corresponding authors.
E-mail addresses: darabid1@gmail.com (M.A. Dar), kowsarmajid@rediffmail.com (K. Majid).
Peer review under responsibility of King Saud University.

Production and hosting by Elsevier

http://dx.doi.org/10.1016/j.arabjc.2016.12.001

shielding as compared to dielectric attributes. Such a material with high SE demonstrates the potential of these materials for making future microwave shields.

1. Introduction

The rapid growth of electronic devices and telecommunication equipments has evolved the problem of electromagnetic interference (EMI), owing to which the lifetime and competence of the instruments are considerably reduced. This also affects the safety operation of many electronic devices. It occurs due to the mutual and unintentional interaction of electromagnetic radiation emitted from the electronic devices (Dar et al., 2012a; Singh et al., 2011). For this purpose, current research is focussed on the design and synthesis of new materials. That can act as shield for such emissions so as to mitigate EMI to ensure uninterrupted performance of gadgets and to avoid its harmful effects on humans. The primary mechanism to EMI shielding is reflection for which the material needs to be conducting. Metal based materials were therefore of premier use but owing to their high density, corrosion susceptibility, uneconomic processing and low specific shielding effectiveness, their use is a matter of debate (Saini and Arora, 2012; Xie et al., 2013). The secondary mechanism is absorption, which demands the material to possess electric and magnetic dipoles so as to interact with electric and magnetic fields of incident radiation. For this purpose, material needs to have a high value of dielectric constant and magnetic permeability. Such materials include ferroelectrics and ferrites respectively. Because of their high density and poor processing, their use has not been much impressive. In addition to above two mechanisms, one more mechanism is the multiple internal reflections to shielding for which the material should be nano sized (Najar and Majid, 2015; Kumar et al., 2014; Dar et al., 2012b; K. Singh et al., 2013). On the other hand, conducting polymers with finite conductivity and non-transparency to microwaves are found to offer an attractive solution. Particularly, synthetic metals such as polyaniline (PANI) based composites have received special attention due to tunable conductivity, adjustable permittivity or permeability, low density, non-corrosiveness, nominal cost, and good thermal and environmental stability resulting in a wealth of techno-commercial applications (Saini et al., 2012; Tantawy et al., 2013; Joseph et al., 2015; Wang et al., 2013; Liu et al., 2016).

In view of above, a core-shell structured PANI/$Li_{0.5}Fe_{2.5-x}Gd_xO_4$ ($0.0 \leqslant x \leqslant 0.2$) nanocomposite material has been prepared by surfactant assisted in situ emulsion polymerization of aniline monomer for the investigation of its EMI shielding properties. An effect of Gd ion doping on the electromagnetic properties of PANI/$Li_{0.5}Fe_{2.5}O_4$ ferrite nanocomposites has also been investigated. It has been found that a very high value of shielding effectiveness has been obtained in the present system than many other systems reported, thereby paving way for its use in practical applications.

2. Experimental

2.1. Synthesis of $Li_{0.5}Fe_{2.5-x}Gd_xO_4$ ($0.0 \leqslant x \leqslant 0.2$) nanoparticles

$Li_{0.5}Fe_{2.5-x}Gd_xO_4$ ($0.0 \leqslant x \leqslant 0.2$) ferrite nanoparticles have been prepared by sol-gel auto combustion method. The mechanistic details are shown in Scheme 1 in which citric acid has been used as capping agent to control the particle size of the given ferrite. However, redundancy in the Gd^{3+} ions occurs at $x = 0.2$ owing to the formation of new phase as has been reflected in its XRD pattern. It means the amount of Fe^{3+} ions substituted by Gd^{3+} ions has a limit for doping in $Li_{0.5}Fe_{2.5-x}Gd_xO_4$ ferrite. This has already been described in our earlier published work (Dar et al., 2016).

2.2. Surfactant assisted synthesis of core-shell structured PANI/$Li_{0.5}Fe_{2.5-x}Gd_xO_4$ ($0.0 \leqslant x \leqslant 0.2$) nano-composite

PANI/$Li_{0.5}Fe_{2.5-x}Gd_xO_4$ ($0.0 \leqslant x \leqslant 0.2$) nanocomposite has been prepared by surfactant assisted in situ oxidative chemical polymerization using ammonium persulfate as oxidant in aqueous medium. The synthetic procedure adopted is as per the literature (Dar et al., 2012a). The nano-crystals of $Li_{0.5}Fe_{2.5-x}Gd_xO_4$ ($0.0 \leqslant x \leqslant 0.2$) ferrite prepared above have been homogenized in 0.3 M aqueous solution of dodecyl benzene sulfonic acid (DBSA) to form a whitish brown emulsion solution. An appropriate amount of aniline (0.1 M) was added to the above solution and again homogenized for 2 h to form micelles of aniline with $Li_{0.5}Fe_{2.5-x}Gd_xO_4$ ($0.0 \leqslant x \leqslant 0.2$) nano-crystals. The micellar structure of aniline was then polymerized by oxidative polymerization using ammonium persulfate ($(NH_4)_2S_2O_8$ (0.1 M)) as oxidant at nearly 5 °C with continuous stirring. During stirring, solution appeared green indicating the successful polymerization of aniline monomer, and thereby nanocomposite formation. After 12 h of stirring, the product so obtained was demulsified by treating with an equal amount of isopropyl alcohol. The precipitates were filtered out and washed with methanol and then dried at 60 °C. This is graphically shown in Scheme 2. Several nanocomposites of PANI with different compositions of $Li_{0.5}Fe_{2.5-x}Gd_xO_4$ ($x = 0.0$, 0.05, 0.10, 0.15 and 0.2) in the same weight of PANI/Ferrite (4:1) have been obtained. Besides this, pure polyaniline doped with DBSA was also synthesized for their comparative study.

3. Results and discussion

3.1. Structural and morphological features of nanocomposite

The X-ray diffraction (XRD) of ferrite particles clearly shows a single phase spinal structure with characteristic peaks corresponding to the planes (210), (220), (311), (400), (421), (422), (511) and (440) as shown in the inset of Fig. 1. However a secondary phase formation occurs at $x = 0.2$ corresponding to $GdFeO_3$, indicating limit to Gd^{3+} doping. The lattice parameter values obtained were found to be in the expected range of the lattice parameter of cubic spinel ferrites. The lattice parameter increases with the increase in Gd ion concentration as shown in Table 1. The diffraction peaks obtained in the XRD pattern are broader, which indicates the nanosized characteristics of the prepared ferrites. The average crystallite size of the samples was estimated from X-ray diffraction peak broadening using Scherrer formula. With

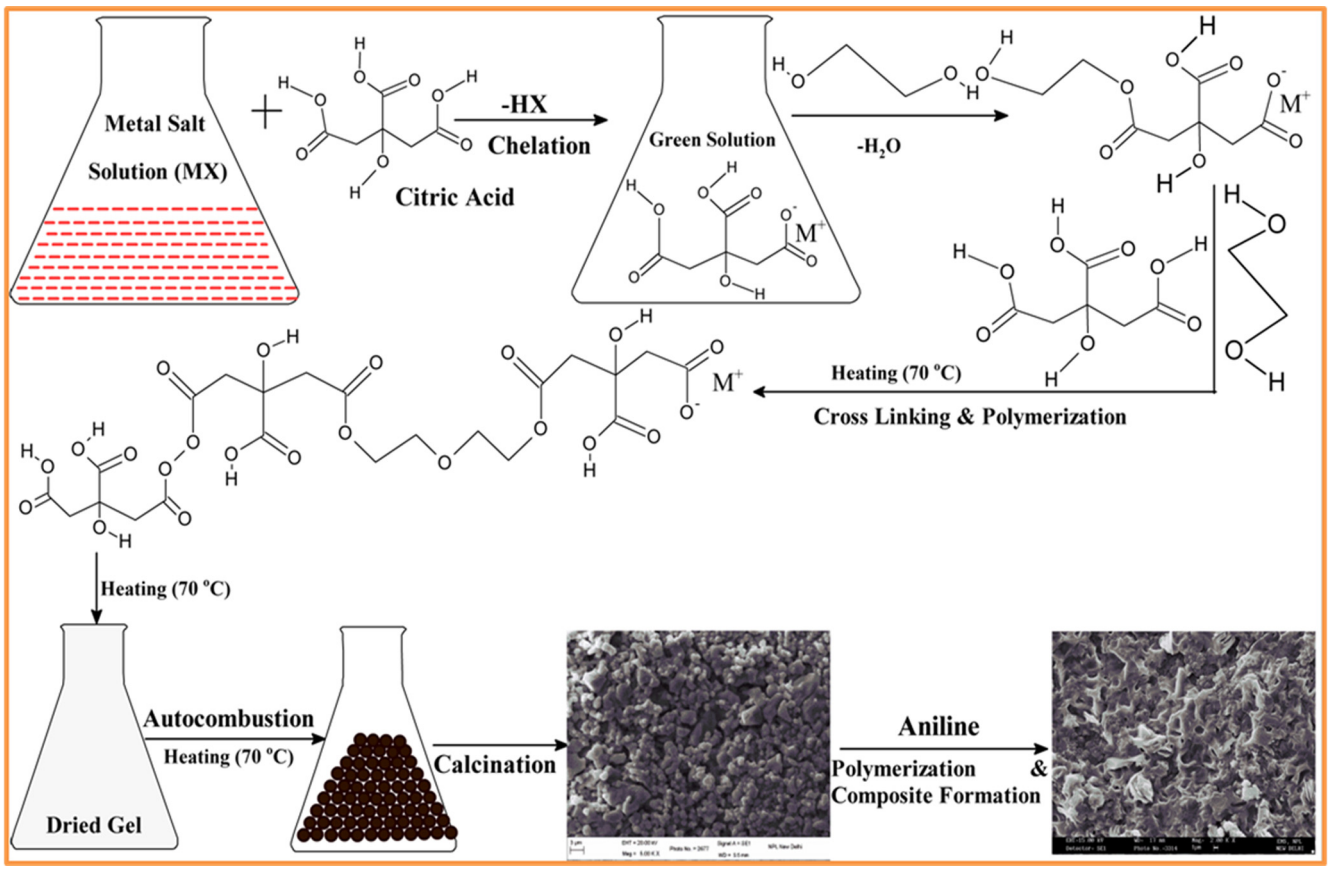

Scheme 1 Schematic representation for the synthesis of $Li_{0.5}Fe_{2.5-x}Gd_xO_4$ ferrite nano-crystals by citrate gel auto combustion method.

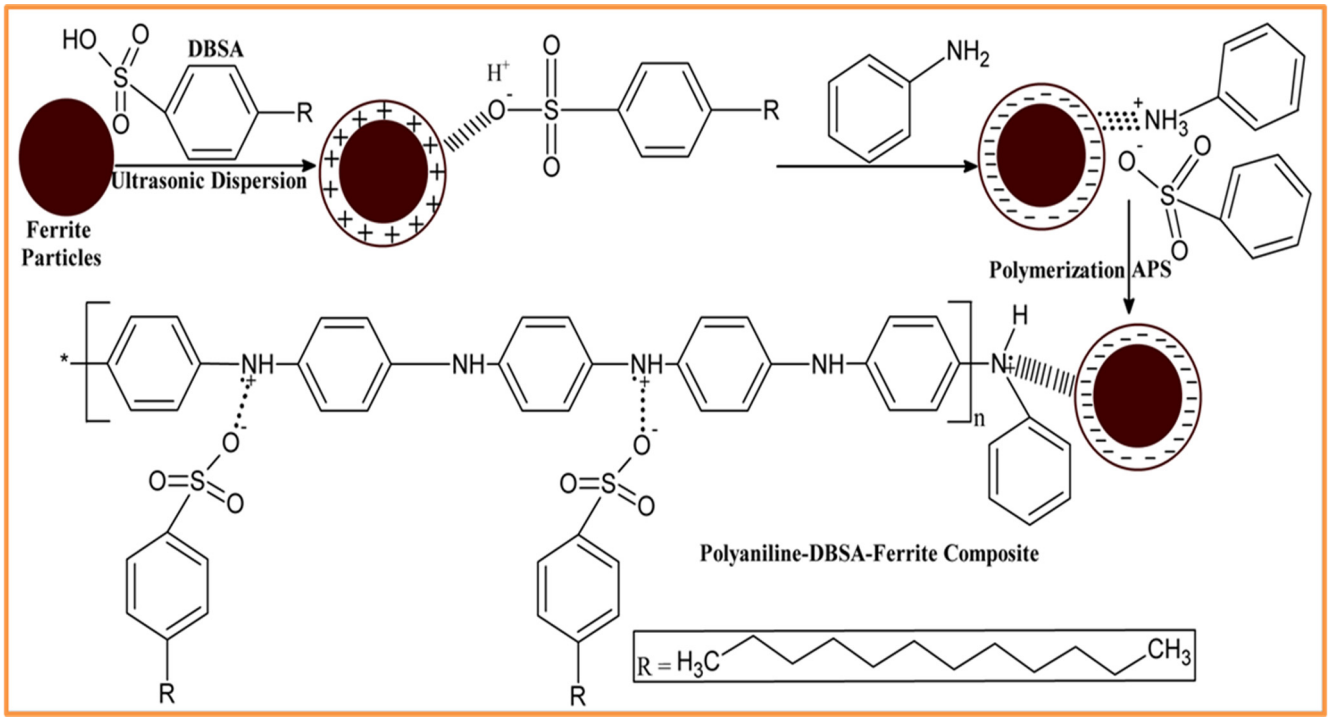

Scheme 2 Schematic representation for synthesis of PANI/$Li_{0.5}Fe_{2.5-x}Gd_xO_4$ nano-composites using in situ emulsion polymerization.

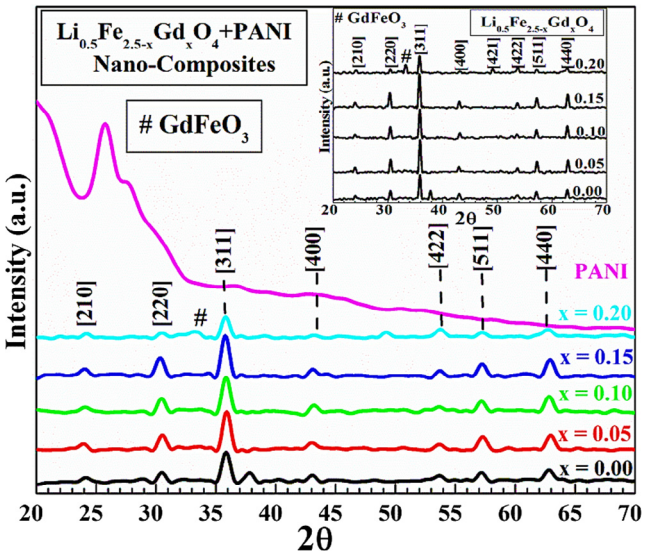

Figure 1 XRD pattern of all the samples of PANI/$Li_{0.5}Fe_{2.5-x}Gd_xO_4$ nano-composites and inset shows the XRD pattern of $Li_{0.5}Fe_{2.5-x}Gd_xO_4$ ferrites.

doping the average crystallite sizes were found to increase from 25.2 to 31.1 nm as shown in Table 1 (Dar et al., 2016). The X-ray diffraction pattern of PANI/$Li_{0.5}Fe_{2.5-x}Gd_xO_4$ nano-composites is shown in Fig. 1. The broad diffraction peaks centered at $2\theta = 20.1°$ and 25.7° can be ascribed to the periodicity parallel and perpendicular to the polymer chains. It indicated that the resulting polymer (PANI) was in the form of highly doped emeraldine salt and had good crystallinity. It is clearly evident that both the characteristic peaks of PANI centered at around $2\theta = 20.1°$ and 25.7° and $Li_{0.5}Fe_{2.5-x}Gd_xO_4$ ferrite nanocrystals appear in the XRD patterns of the nano-composites. The intensities of the characteristic peaks of PANI became weaker after introducing ferrite nanocrystals into the polymer matrix, revealing the decrease in the concentration of PANI in the nano-composite. The peak broadening has also been found on introducing PANI into the ferrite matrix. It may be attributed to the amorphous nature of PANI, which overwhelms the crystalline nature of $Li_{0.5}Fe_{2.5-x}Gd_xO_4$ ferrite nanocrystals. The presence of a conducting shell encapsulating the magnetic nanocrystals is helpful for the proper impedance matching. It is necessary for enhancing the absorption of the electromagnetic waves.

SEM images of ferrite nano particles exhibit granular morphology with a grain size in the range of 280–370 nm for different compositions as shown in Table 1. SEM images have also indicated that with the increase in Gd ion concentration, the density increases and porosity decreases. The increase in Gd content led to the increase in average grain size up to $x = 0.15$. However, the average grain size for sample with $x = 0.20$ decreases (Dar et al., 2016). Fig. 2 shows the SEM images of PANI and PANI/$Li_{0.5}Fe_{2.5-x}Gd_xO_4$ ferrite nano-composites. It is evident that polyaniline exhibits continuous morphology, while in nano-composites there is clearly a secondary phase due to ferrite particles. A change in the ferrite composition by different Gd^{3+} content viz $x = 0.0$, 0.1, 0.15 and 0.2 changes the surface morphology of corresponding nanocomposite. This is owing to the change in the grain size of ferrite particles which is clearly reflected in nano-composites. Moreover, a cross linked network type structure has been envisioned in the nano-composites as observed from SEM images.

The TEM micrographs of $Li_{0.5}Fe_{2.5-x}Gd_xO_4$ ferrite nanocrystals doped with different concentrations of Gd ion ($x = 0.05$ and 0.10) are presented in the inset of Fig. 3. The average size of the particles for these two compositions was found to be in the range of 22–31 nm and 24–32 nm, which are in good agreement with that obtained by XRD measurements (Dar et al., 2016). Also, an obvious agglomeration of particles has been observed which can be either due to the nano size of particles or the presence of magnetism. Nano-composites on the other hand clearly exhibit a core-shell type structure in which ferrite particles act as dark core and PANI as light shell owing to different penetrability. These core-shell structured particles are interconnected to one another through PANI chains thereby supporting SEM (Fig. 2). In comparison with the uncoated ferrite particles, the PANI formed on the surface of ferrite particles leads to the increase in the particle size as is evident from Fig. 3. The average size of particles in both the nano-composites ($x = 0.05$ and 0.10) was found to be approximately 25.3–33.8 nm and 26.2–37.8 nm respectively. Such results are in consistent with PANI/$Mn_{0.5}Zn_{0.5}Fe_2O_4$ prepared by same method as reported in the literature (Dar et al., 2012a).

3.2. Magnetic properties

The magnetic hysteresis loops for $Li_{0.5}Fe_{2.5-x}Gd_xO_4$ ($0.0 \leqslant x \leqslant 0.2$) ferrites were measured using vibrating sample magnetometer (VSM) as shown in inset of Fig. 4. The value of saturation magnetization obtained from the curves was found to increase with Gd doping up to $x = 0.15$. The saturation magnetization obtained at room temperature has been increased from 44.5 emu/g to 69.6 emu/g due to the doping of Gd^{3+} ions in $Li_{0.5}Fe_{2.5-x}Gd_xO_4$ ferrite. However a small

Table 1 Various structural and magnetic parameters of $Li_{0.5}Fe_{2.5-x}Gd_xO_4$ and PANI/$Li_{0.5}Fe_{2.5-x}Gd_xO_4$ ferrite nano-composites.

Composition (x)	Lattice parameter (Å)	Crystallite size (nm) (D_{XRD})	Grain size (nm) (D_{SEM})	M_S (emu/g)	
				Ferrite	Composite
0.00	8.316	25.2	280	44.5	20.6
0.05	8.331	27.9	324	50.1	28.6
0.10	8.345	29.7	359	58.9	32.4
0.15	8.367	31.1	404	69.	35.2
0.20	8.379	28.1	372	30.9	13.4

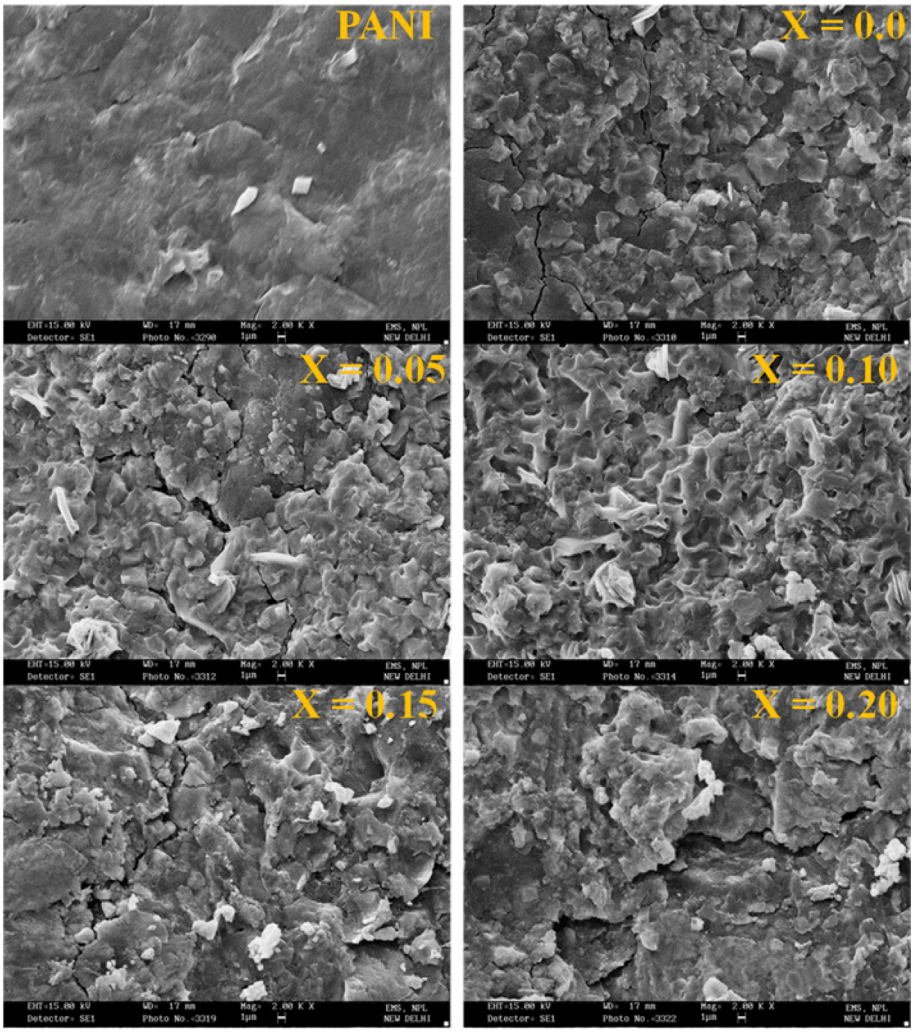

Figure 2 SEM micrographs of PANI and PANI/$Li_{0.5}Fe_{2.5-x}Gd_xO_4$($0.0 \leqslant x \leqslant 0.2$) ferrite nano-composites.

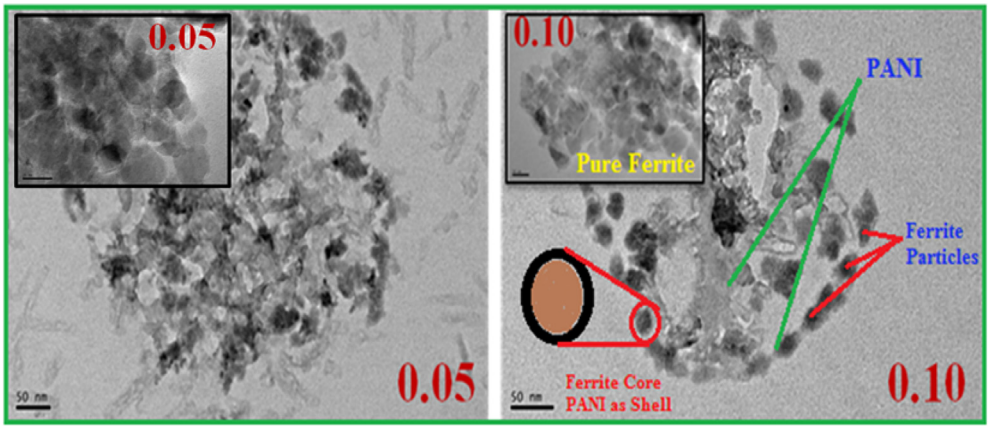

Figure 3 TEM micrographs of PANI/$Li_{0.5}Fe_{2.5-x}Gd_xO_4$ ($x = 0.05$ and 0.10) ferrite nano-composites.

value of saturation magnetization has been obtained for sample with $x = 0.20$. This increase in saturation magnetization has been attributed to the higher magnetic moment associated with Gd^{3+} ions in comparison with Fe^{3+} ions. Saturation magnetization is also influenced by extrinsic factors such as microstructure, grain size and porosity of the material. The formation of magnetic domain walls becomes easy on increasing grain size. Hence, the value of saturation magnetization increases due to the domain wall movement under the action of an applied magnetic field. The gradual increase in average

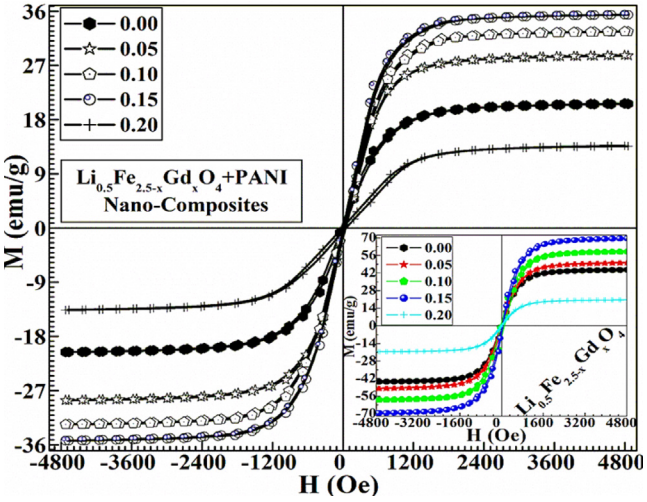

Figure 4 M-H curves of PANI/$Li_{0.5}Fe_{2.5-x}Gd_xO_4$ ($0.0 \leqslant x \leqslant 0.2$) ferrite nano-composites and inset shows the M-H curves of $Li_{0.5}Fe_{2.5-x}Gd_xO_4$ ferrites.

crystallite size with the addition of Gd ions, agrees well with the increase in saturation magnetization. Also, it can be attributed to the decrease in porosity from $x = 0.0$ to $x = 0.15$. A low value of saturation magnetization (27 emu/g) has been obtained for the sample with $x = 0.2$. This can be attributed to the secondary phase formation, which dilutes the magnetic structure. It can also be attributed to the decrease in grain size (Dar et al., 2016). The core-shell structured PANI/$Li_{0.5}Fe_{2.5-x}Gd_xO_4$ ferrite nanocomposite exhibits similar magnetic behavior as shown in Fig. 4. The value of saturation magnetization obtained for PANI/$Li_{0.5}Fe_{2.5-x}Gd_xO_4$ ferrite nanocomposites was reduced in comparison with pure ferrite samples as shown in Table 1. This is still a very high value (35 emu/g for $x = 0.15$) and is therefore useful for the attenuation of electromagnetic waves via absorption losses. Such a high value of saturation magnetization has been attributed to the prevention of free magnetic spin orientation available on the ferrite surface owing to the development of hydrogen bonding between —O— of ferrite and —N— atom of polyaniline. This can also lead to the reduction in particle-particle exchange interaction, thereby allowing easy alignment of magnetic spins with the applied magnetic field (Dar et al., 2012a). Furthermore, retention of magnetization in PANI coated ferrite has been observed with reduced magnetization, compared to pure ferrite. This has been attributed to the presence of non-magnetic PANI in the magnetic ferrite matrix. These results are in consistent with SEM and TEM results.

3.3. Electromagnetic interference (EMI) shielding performance of the prepared core-shell structured nano-composite

Electromagnetic interference (EMI) shielding refers to the reflection and/or absorption of electromagnetic radiation by a material, which thereby acts as a shield against the penetration of the radiation through the shield. This is expressed by measuring the shielding effectiveness (SE) of the shield material, which is defined as the ratio of residual energy to the impinging energy. This is equivalent to the electromagnetic radiation transmitted (subscript T) through the shield divided by the incident (subscript I) wave and can be calculated from any of the energy intensities viz electric (E), magnetic (H) and electromagnetic power (P) using relation (I):

$$SE_T(dB) = -10\log\frac{E_T}{E_I} = -10\log\frac{H_T}{H_I} = -10\log\frac{P_T}{P_1} \quad \text{(I)}$$

The attenuation of electromagnetic radiation can be owing to (1) reflection losses from the front face of material, for which the material needs to be conducting (2) absorption losses which demand the material to be dielectric and magnetic in nature and (3) multiple internal reflections, for which the material should be nano sized, and is usually significant in thin shields. Thus for a shielding material, the total shielding effectiveness (SE_T) is given by relation (II):

$$SE = SE_R + SE_A + SE_M \quad \text{(II)}$$

where SE_R and SE_A are the shielding effectiveness owing to the reflection and absorption losses and are given by using relation (III) and (IV) respectively:

$$SE_R(dB) = 10\log\frac{\sigma_{ac}}{16\omega\mu_r\mu^{\circ}} \quad \text{(III)}$$

$$SE_A(dB) = 20(d/\delta)\log e = 20d\sqrt{\frac{\omega\mu_r\sigma_{ac}}{2}}\log e \quad \text{(IV)}$$

where d is the thickness of the shield, μ_r is the magnetic permeability, δ is the skin depth, $\sigma_{ac} = \omega\varepsilon_o\varepsilon''$ is the frequency dependent conductivity, ε'' is the imaginary part of permittivity, ω is the angular frequency, and ε_o is the permittivity of the free space. SE_M is the shielding effectiveness due to the multiple internal reflections. It is usually neglected, when absorption loss is greater than 10 dB (Reshi et al., 2015). In this study, the EMI Shielding effectiveness of PANI/$Li_{0.5}Fe_{2.5-x}Gd_xO_4$ ($0.0 \leqslant x \leqslant 0.2$) nanocomposite measured with a thickness of 2 mm in the X-band (8–12 GHz) frequency range has been performed. The EMI shielding effectiveness was found to show weak field dependence for all the samples as is evident from Fig. 5. The larger value of SE_R and SE_A reflects the high shielding effectiveness of nanocomposite than pristine PANI. Among the nano-composites, a higher value of SE_R (5.1 dB) and SE_A (35.2 dB) has been observed for sample with $x = 0.0$. On further doping of Gd^{3+} ions in $Li_{0.5}Fe_{2.5}O_4$ ferrite, both the values were found to decrease. However for the sample with $x = 0.02$, the values of SE_R (6 dB) and SE_A (36 dB) are exceptionally high. The absorption loss mechanism to shielding was found to be a dominant factor over the reflection loss. This is clearly reflected in the total shielding effectiveness of the nanocomposite material as shown in Fig. 5(d, c). A higher value (42 dB) of total shielding effectiveness for the present nanocomposite has been observed than many other systems reported as shown in the Table 2 (Dar et al., 2012a; Tantawy et al., 2013; Wang et al., 2013; Kumar et al., 2015; A.P. Singh et al., 2013; Shen et al., 2013; Zhang et al., 2011).

The above stated observations can be explained by the fact that DBSA doped PANI exhibits lower conductivity owing to the formation of localized charges (polarons and bipolarons) leading to the strong divergence and relaxation effect. This is responsible for its dominant absorption over reflection (Gupta et al., 2014). Since ferrite nanoparticles being dielectric and magnetic in nature, their addition in PANI matrix leads to enhancement in the magnetic and dielectric attributes of the

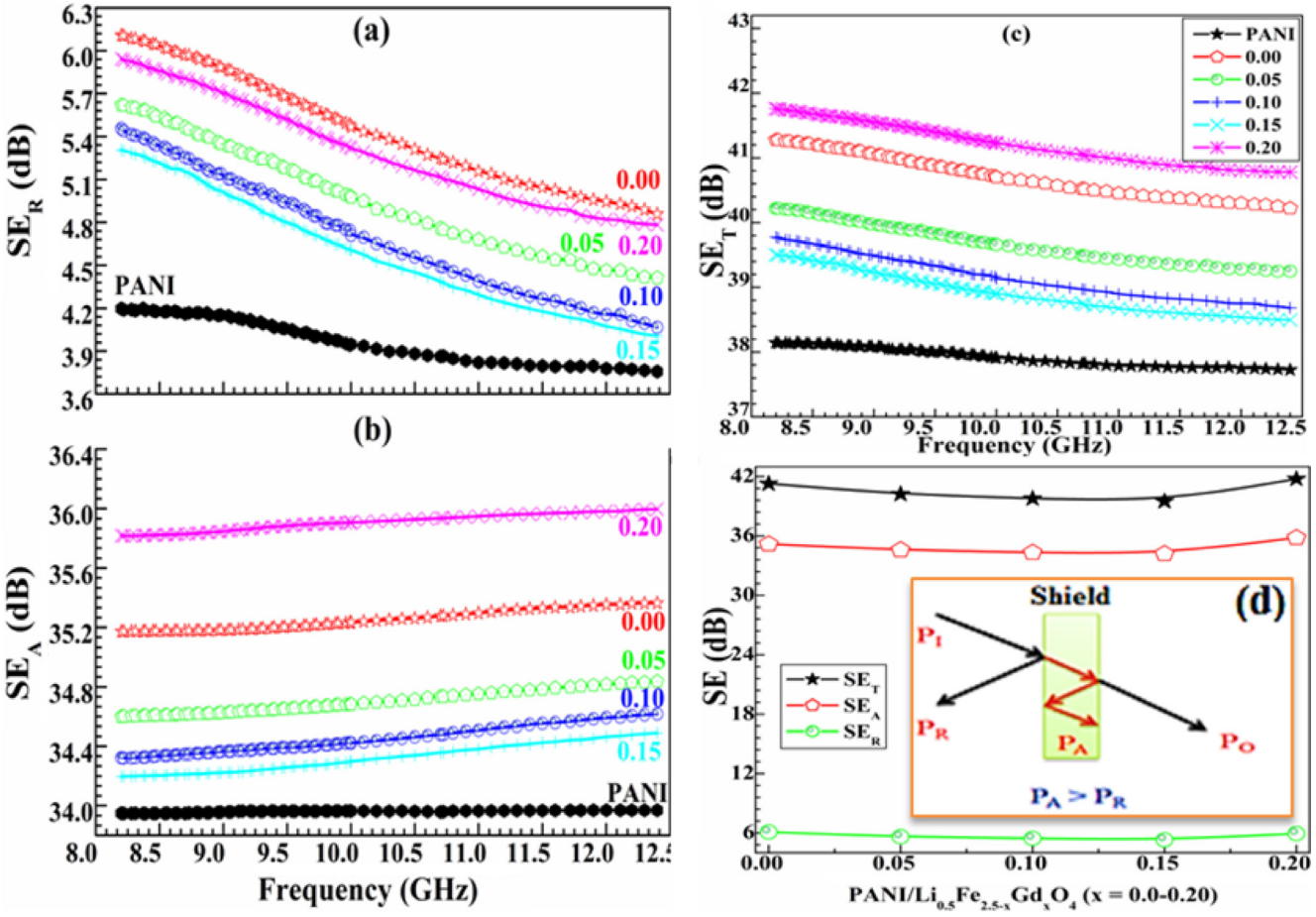

Figure 5 Variation of shielding effectiveness SER (a), SEA (b), and SET (c) with frequency in 8.2–12.4 GHz, and variation of shielding effectiveness with composition (d).

Table 2 Comparison of total shielding effectiveness of different composites in the frequency range of 8–12 GHz.

System	SE_T (dB)	References
PANI/$Li_{0.5}Fe_{2.5-x}Gd_xO_4$ ($0.0 \leqslant x \leqslant 0.2$)	42	Present work
PANI/$Mn_{0.5}Zn_{0.5}Fe_2O_4$	32	Dar et al. (2012a)
HCl-doped polyaniline	18	Tantawy et al. (2013)
PANI/$Mn_{0.5}Zn_{0.5}Fe_2O_4$	20	Wang et al. (2013)
Polyaniline/carbon fiber	35	Kumar et al. (2015)
Multi-walled carbon nanotube/Portland cement composites	28	Singh et al. (2013)
Polyetherimide/graphene@Fe_3O_4	41.5	A.P. Shen et al. (2013)
Polymethylmethacrylate (PMMA)/graphene nanocomposite	19	Zhang et al. (2011)

nanocomposite material. This helps in the attenuation of electromagnetic radiations via absorption losses, since it depends on the electric and magnetic dipoles that can interact with the electromagnetic radiation (Verma et al., 2015). In order to establish correlation between observed shielding response and electromagnetic attributes, complex permittivity (ε^*) and permeability (μ^*) values of samples were also calculated from experimental scattering parameters using the Nicolson-Ross-Weir algorithm (Saini and Arora, 2013). The complex permittivity (ε^*) of the nanocomposite shows that both the real (ε') and imaginary (ε'') permittivity exhibits decreasing trend with increasing frequency as shown in Fig. 6(a, b). This has been attributed to the inability of the dipoles in nanocomposite to follow the applied field. Moreover, nanocomposites show better dielectric properties than pristine PANI. This is owing to the Maxwell-Wagner type interfacial polarization as there is a significant difference between the electrical conductivity of PANI matrix and ferrite nanoparticles. On increasing the content of Gd^{3+} ions from $x = 0.0$ to 0.15, the dielectric attributes decrease. It can be due to the increase in crystallite

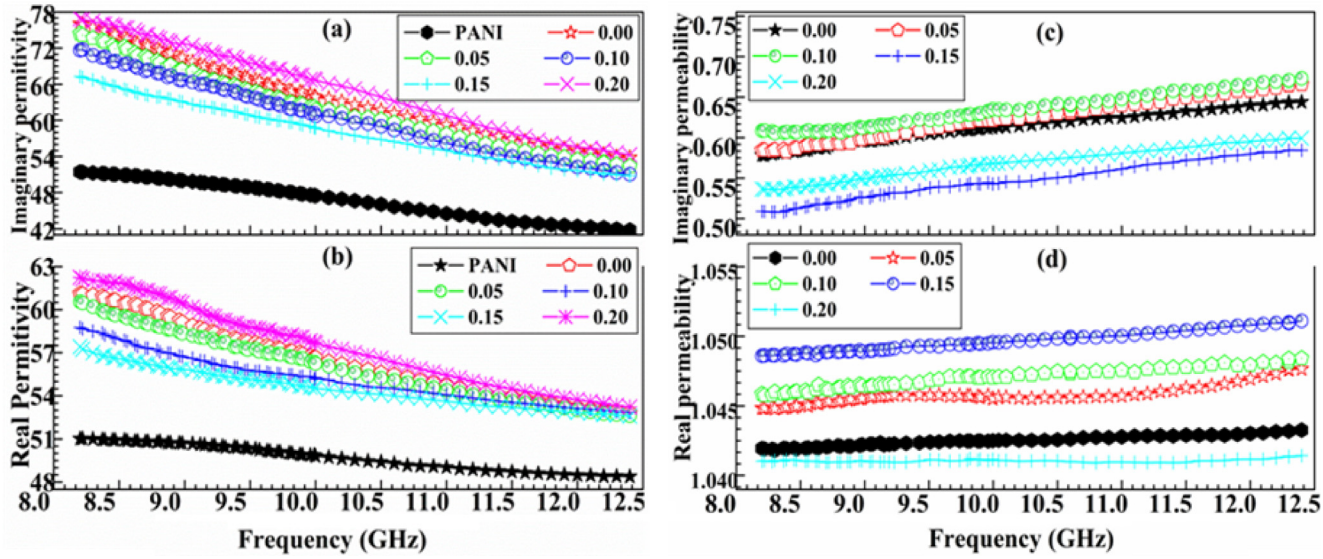

Figure 6 Variation of imaginary permittivity (a), real permittivity (b), imaginary permeability (c) and real permeability with frequency in 8.2–12.4 GHz range.

size. This intern decreases the number of grain boundaries and hence the interfacial polarization also decreases. However, the higher value of dielectric constant and dielectric loss associated with $x = 0.20$ sample can be due to the decrease in crystallite size. The complex permeability (μ^*) of PANI/$Li_{0.5}Fe_{2.5-x}Gd_xO_4$ ferrite nano-composites is shown in Fig. 6(c, d). The magnetic permeability has been found to increase with increasing Gd^{3+} ion content in PANI/$Li_{0.5}Fe_{2.5-x}Gd_xO_4$ ferrite nano-composite. This is on account of increased particle size, which leads to the facile formation of magnetic domain walls thereby showing better magnetic properties. A lower value of magnetic permeability for $x = 0.20$ sample can be due to its small size. Furthermore, on increasing frequency of applied field (H), the induced magnetization (B) lags behind the applied field giving rise to anisotropic effects (magneto-crystalline anisotropy and shape anisotropy). These anisotropic effects become much stronger at nanoscale level. This is responsible for magnetic losses in the magnetic material. An increase in crystallite size from $x = 0.0$–0.15 clearly reflects a decrease in the anisotropic effects, and hence the magnetic losses. These results are in consistent with the results discussed in Section 3.1 (Dar et al., 2016). Because of this increased complex permeability and permittivity, an improvement in the equality of electromagnetic attributes takes place. This results into the better impedance matching which in turn improves absorption of the electromagnetic microwave. It also helps in the decrease of surface reflection in the material as is evident from SE_R values.

4. Conclusions

Successful synthesis of a core-shell structured PANI/$Li_{0.5}Fe_{2.5-x}Gd_xO_4$ ($0.0 \leqslant x \leqslant 0.2$) ferrite nanocomposite has been prepared by surfactant assisted in situ emulsion polymerization of aniline monomer for the investigation of EMI shielding in X-band. It has been found that the present nanocomposite material exhibits a higher value (42 dB) of total SE than many other systems reported. The main contributing factor has been ascribed to the absorption (SE_A = 34–36 dB) instead of reflection (SE_R = 4.0–6.3 dB), owing to the enhancement in the electromagnetic attributes. An effect of Gd^{3+} ion content on PANI/$Li_{0.5}Fe_{2.5-x}Gd_xO_4$ nanocomposite has been analyzed for the electromagnetic attenuation. It was observed to decrease with Gd^{3+} doping, except for $x = 0.2$ sample. This has been attributed to the increasing particle size of ferrites, resulting into the decrease in dielectric ($\varepsilon' = 59$–56 at 9.5 GHz) attributes owing to increased grain to grain contact. Higher value of SE for $x = 0.2$ sample can be due to the secondary phase formation in ferrite, which increases the number of grain boundaries and thereby increases ε'. However, increase in magnetization with increasing Gd^{3+} is less likely a factor affecting shielding as compared to dielectric attributes. Such a material with high SE is conducive for practical applications.

Note

The authors declare no competing financial interest.

Acknowledgments

M. Abdullah Dar is thankful to Council of Scientific and Industrial Research (CSIR), New Delhi, India, for their financial assistance to carry out this research work under grant No. 9/984 (0002) 2K14-EMR-I. M. Abdullah Dar and Kowsar Majid are also grateful to Prof. Rajat Gupta, Director, NIT Srinagar, for providing constant encouragement and motivation to carry out this work. Help and support from Dr. T. Ara, Head, Department of Chemistry is also acknowledged.

References

Dar, M.A., Kotnala, R.K., Verma, V., Shah, J., Siddiqui, W.A., Alam, M., 2012a. J. Phys. Chem. C 116, 5277–5287.
Dar, M.A., Shah, J., Siddiqui, W.A., Kotnala, R.K., 2012b. J. Alloys Compd. 523, 36–42.
Dar, M.A., Majid, K., Najar, M.H., Kotnala, R.K., Shah, J., 2016. Mater. Des. 90, 443–452.
Gupta, T.K., Singh, B.P., Mathur, R.B., Dhakate, S.R., 2014. Nanoscale 6, 842–851.

Joseph, N., Varghese, J., Sebastian, M.T., 2015. RSC Adv. 5, 20459–20466.
Kumar, R., Singh, A.P., Chand, M., Pant, R.P., Kotnala, R.K., Dhawan, S.K., Mathur, R.B., Dhakate, S.R., 2014. RSC Adv. 4, 23476–23484.
Kumar, R., Joon, S., Singh, A.P., Singh, B.P., Dhawan, S.K., 2015. Am. J. Poly. Sci. 5, 28–39.
Liu, Q., Jing, S., Wang, S., Zhuo, H., Zhong, L., Peng, X., Sun, R., 2016, 4, 13352–13362.
Najar, M.H., Majid, K., 2015. RSC Adv. 5, 107209–107221.
Reshi, H.A., Singh, A.P., Pillai, S., Yadav, R.S., Dhawan, S.K., Shelke, V., 2015. J. Mater. Chem. C 3, 820–827.
Saini, P., Arora, M., 2012. In: Gomes, A.D. (Ed.), New Polymers for Special Applications. Intech, Croatia, pp. 71–112.
Saini, P., Arora, M., 2013. J. Mater. Chem. A 1, 8926–8934.
Saini, P., Choudhary, V., Vijayan, N., Kotnala, R.K., 2012. J. Phys. Chem. C 116, 13403–13412.
Shen, B., Zhai, W., Tao, M., Ling, J., Zheng, W., 2013. Appl. Mater. Interfaces 5, 11383–11391.
Singh, B.P., Prabha, Saini, P., Gupta, T., Garg, P., Kumar, G., Pande, I., Pande, S., Seth, R.K., Dhawan, S.K., Mathur, R.B., 2011. J. Nanopart. Res. 13, 7065–7074.
Singh, A.P., Gupta, B.K., Mishra, M., Govind, Chandra, A., Mathur, R.B., Dhawan, S.K., 2013. Carbon 56, 86–96.
Singh, K., Ohlan, A., Pham, V.H., Balasubramaniyan, R., Varshney, S., Jang, J., Hur, S.H., Choi, W.M., Kumar, M., Dhawan, S.K., Kong, B.S., Chung, J.S., 2013. Nanoscale 5, 2411–2420.
Tantawy, H.R., Aston, D.E., Smith, J.R., Young, J.L., 2013. Appl. Mater. Interfaces 5, 4648–4658.
Verma, M., Singh, A.P., Sambyal, P., Singh, B.P., Dhawan, S.K., Choudhary, V., 2015. Phys. Chem. Chem. Phys. 17, 1610–1618.
Wang, W., Gumfekar, S.P., Jiao, Q., Zhao, B., 2013. J. Mater. Chem. C 1, 2851–2859.
Xie, S., Guo, X.N., Jin, G.Q., Guo, X.Y., 2013. Phys. Chem. Chem. Phys. 15, 16104–16110.
Zhang, H.B., Yan, Q., Zheng, W.G., He, Z., Yu, Z.Z., 2011. ACS Appl. Mater. Interfaces 3, 918–924.